THE ASTROPHYSICAL JOURNAL, 312:50–65, 1987 January 1

HIGH-RESOLUTION SPECTROSCOPY OF THE $z = 1.79$ ABSORPTION-LINE SYSTEM TOWARD B2 1225+317[1]

JILL BECHTOLD
Steward Observatory, University of Arizona and Mount Wilson and Las Campanas Observatories of the Carnegie Institution of Washington

RICHARD F. GREEN
Kitt Peak National Observatory, National Optical Astronomy Observatories[2]

AND

D. G. YORK
Astronomy and Astrophysics Center, University of Chicago
Received 1985 December 12; accepted 1986 June 13

ABSTRACT

We observed several species of the absorption line system at $z = 1.79$ toward the bright quasar B2 1225+317 ($z_{em} = 2.22$, $m_v = 15.9$) with the echelle spectrograph on the Multiple Mirror Telescope, at a resolution of 10 km s^{-1}. The absorption-line profiles differ from species to species, with some velocity components showing absorption in both low-ionization species (Mg I, Mg II, Fe II, Si II, C II) and high-ionization species (C IV and Si IV), while other components show absorption only in C IV and Si IV. The relative column densities of Si II, Mg II, Zn II, Fe II, and H I are consistent with the local interstellar medium values, within the uncertainties. We investigated the properties of the radiation field longward of the Lyman limit with the Mg I/Mg II, C I/C II, and Si II/Si IV ratios, along with a density estimate from a limit on the C II/C II* ratio ($\log n < -1$ cm^{-3}). We find that, in the context of our models, the specific intensity at 1000 Å is in the range $-19.9 < \log J_\nu < -19.1$ ergs s^{-1} cm^{-2} Hz^{-1}, consistent with estimates of the near-UV radiation field in the halo of a spiral galaxy.

Subject heading: quasars

I. INTRODUCTION

B2 1255+317 is a bright ($m_v = 15.9$), high-redshift ($z_{em} = 2.22$) QSO, with a prominent metal-containing absorption-line system at $z_{abs} = 1.79$. The absorption system was first identified by Ulrich (1976), who commented that B2 1225+317 "affords an exceptional opportunity for detailed study." Subsequent studies at moderate spectral resolution were carried out by Wilkerson *et al.* (1978), Grandi (1979), and Sargent *et al.* (1980). The presence of strong lines from a range of ionization states of several elements, the large difference between z_{abs} and z_{em}, and early evidence that the line profiles are complex, indicated that it is an example of absorption arising in material associated with an intervening galaxy. The comparison of the properties of this and similar high-redshift quasar absorption-line systems with analogous observations of the Milky Way and other local galaxies can yield unique information about the kinematical and chemical evolution of gas in galaxies.

York *et al.* (1984; hereafter Paper I) presented a spectrum of the $z = 1.79$ C IV doublet obtained with the Multiple Mirror Telescope (MMT) echelle spectrograph. They showed that the profile of C IV, which at 40 km s^{-1} resolution had shown, incipiently, three separate velocity components (Sargent *et al.* 1980; Sargent 1977), split into at least 11 components when observed at very high resolution ($R = 30{,}000$ or $c/R = 10$ km s^{-1}, corresponding to Doppler width $b = 6$ km s^{-1}). Also, Paper I placed upper limits on the b values of several of the velocity components in the range 6–8 km s^{-1}, which corresponds to thermal temperatures of 26,000–46,000 K. These temperatures are cooler than the temperatures at which observable C IV is likely to be produced by collisional ionization: the ionization fraction of C IV peaks at $T = 10^5$ K for collisional ionization equilibrium and is less than 3×10^{-5} for $T < 46{,}000$ K (Shull and Van Steenberg 1982). Paper I concluded therefore, that for these velocity components, photoionization or shock ionization dominates collisional ionization in determining the distribution of ions. By comparison, in our Galaxy, both photoionization (York 1982) and collisional ionization (Savage and Massa 1985) have been suggested as the source of C IV.

In addition, the velocity width of the aggregate C IV profile in the B2 1225+317 system was shown to be about 500 km s^{-1}, which is much larger than the C IV or Si IV profiles observed through the halo of our Galaxy (see discussion in York *et al.* 1986, and references therein). This large width, and the large number of velocity components, have led to the suggestion that in this system and similar complex systems, our line of sight is passing through a cluster of galaxies (Pettini *et al.* 1983; Paper I). The absorption we see is then due to the gaseous halos of several galaxies overlapping in projection, with the large velocity width reflecting the velocity dispersion of the cluster as a whole. Although an unbiased sample of C IV systems observed at high resolution is not yet available, the relatively frequent occurrence of such complex systems in QSO spectra studied so far, compared to the number predicted from the distribution of galaxies and clusters, suggests that statistically, few of the complex systems can, in fact, be attributed to cluster lines of sight. If a majority arise instead in

[1] Based on data obtained at the Multiple Mirror Telescope Observatory, a joint facility of the Smithsonian Institution and the University of Arizona.

[2] NOAO is operated by the Association of Universities for Research in Astronomy, Inc., under contract with the National Science Foundation.

single-galaxy halos, then the implication is that these are not halos similar to our own (see also York *et al.* 1986).

To pursue this comparison of QSO absorption-line systems and the gas in present-day galaxies, we obtained observations of other species in the $z = 1.79$ system toward B2 1225+317 with the MMT echelle spectograph. The advantages of detailed study at echelle resolution are that one can resolve the line widths of the lighter elements, detect weak, unsaturated lines of the less abundant species, and make accurate physical measurements in the closely spaced velocity components. Here we discuss the differences in the line profiles among the different species and attempt to derive abundances and other physical properties of those velocity components which show absorption in the low-ionization species, Mg I, Mg II, and Fe II. The physical conditions in the velocity components which are seen primarily in the high-ionization species, C IV and Si IV, are discussed in a subsequent paper (Bechtold *et al.* 1986*a*, hereafter Paper II).

II. DATA

Observations were made with the Multiple Mirror Telescope (MMT) echelle spectrograph (Chaffee 1974) and intensified Reticon detector (Latham 1982). The wavelength ranges covered, exposure times, and dates of observations are given in Table 1. The spectrograph and telescope operating procedures are detailed in Chaffee *et al.* (1983). A 1″ entrance slit was used, and a resolution of 10 km s^{-1} (FWHM) was achieved. Every 20 min the exposures were stopped and the spectrum of a thorium-argon wavelength standard was recorded. Each exposure was divided by a continuum white-light spectrum to remove pixel-to-pixel variations in sensitivity, and then wavelength corrected. The resulting 20 min accumulations were rebinned, co-added, and dark-subtracted. The residuals of the dispersion polynomials fitted to the thorium-argon lines were typically about 0.3 pixels, or 1.5 km s^{-1}, so that quoted wavelengths are uncertain by that amount. One exception is the spectrum of Mg I λ2852 centered at 7970 Å. Here, the paucity of thorium-argon lines in this region resulted in a substantially larger uncertainty in the dispersion curve, with wavelength errors for each 20 min accumulation on the order of 0.3 Å or 13 km s^{-1}.

The dark level was estimated by several long (2–4 hr) accumulations made periodically during each run, which were smoothed, scaled to exposure time, and subtracted from the data. Since zero-point errors can dominate uncertainties in column densities for weak, unsaturated lines, it is important that the dark level be subtracted with care. The typical dark count was four counts per pixel per second during the February run, and three counts per pixel per second during the April run, with variations of up to 40% during runs due to instabilities in the detector cooling system. In addition, scattered light may affect the zero-point and is difficult to estimate. We estimate the uncertainty in the zero point to be on the order of 30%.

Separate integrations on the star HD 93521 and blank sky were obtained at each setting redward of 5000 Å to identify telluric absorption and emission features, respectively. At other settings, the sky contribution to the flux was negligible, so that sky subtraction was not necessary.

III. ANALYSIS

In Figures 1–10, we plot each co-added, dark-subtracted spectrum, smoothed with a boxcar filter 3 pixels wide. Indicated for each species are the expected positions of the velocity components corresponding to the reddest and bluest C IV components listed in Paper I. Also indicated are the expected positions of strong metal lines corresponding to unidentified lines seen blueward of Lyman-α in emission, under the assumption that they are Lyman-α (Paper II); these predicted metal lines are listed in Table 2. In no case do these latter lines significantly contaminate the profiles of the $z = 1.79$ system. In Table 1 we list an equivalent width limit for any transition in each spectrum. This limit is the equivalent width for which a line of FWHM = 10 km s^{-1} has a reduced $\chi^2 = 5$ with respect to the observed continuum. Mg II or Fe II lines from lower redshift systems could fall in the observed spectral regions, however, and contaminate the $z = 1.79$ profiles.

Voigt profiles were fitted to each line in the $z = 1.79$ system, in order to derive column densities and temperatures of the absorbing material. The analytic approximations given in Humlicek (1979) for the Hjerting functions were used to generate the Voigt profiles. The instrumental profile was taken to be Gaussian with FWHM = 10 km s^{-1}. The atomic parameters adopted are listed in Table 3, and the results of the profile fitting are given in Table 4, except for Si IV $\lambda\lambda$1393, 1403, which will be discussed in Paper II. The number of components, central wavelength of each component, column density, and Doppler width were all varied until a minimum in χ^2 space was found. Fits for members of doublets were forced to give consistent column densities and temperatures for each velocity com-

TABLE 1

LOG OF OBSERVATIONS

Observed Wavelength Range (Å)	Species	Exposure Time (minutes)	Date of Observation	Heliocentric Correction (km s^{-1})	Observed Equivalent Width Limit (mÅ)
3879–3910.....	Si IV λ1397	160	1984 Jun 9	+25.2	
3911–3933.....	Si IV λ1403	280	1984 Feb 8	−14.5	
		210	1984 Apr 24	+16.9	
4245–4282.....	Si II λ1526	120	1984 Apr 23	+16.5	55
4480–4505.....	Fe II λ1608	120	1984 Apr 25	+17.1	40
4615–4650.....	C I λ1657	110	1984 Apr 24	+16.9	140
5639–5685.....	Zn II λ2025	110	1984 Feb 21	−9.2	78
6522–6580.....	Fe II λ2345	120	1984 Feb 9	−14.1	25
7219–7285.....	Fe II λ2600	200	1984 Feb 7	−14.8	50
7798–7866.....	Mg II λ2800	80	1984 Feb 6–7	−15.0	60
7950–7990.....	Mg I λ2852	140	1984 Feb 9	−14.1	78

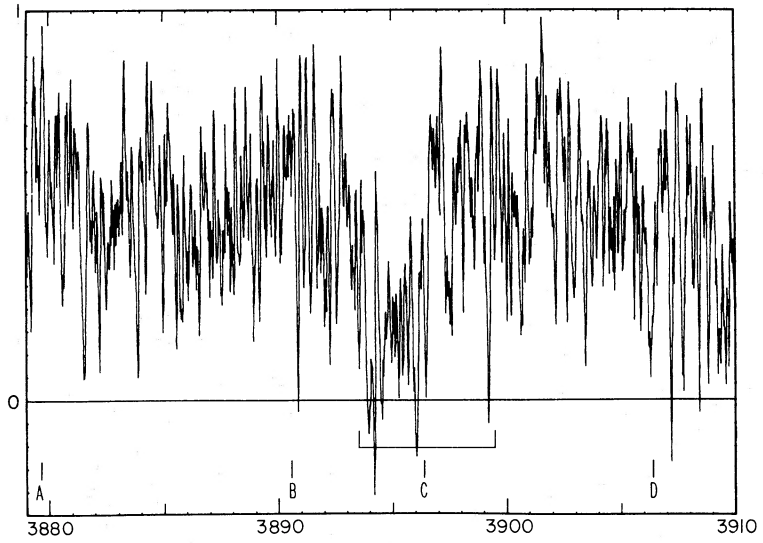

FIG. 1

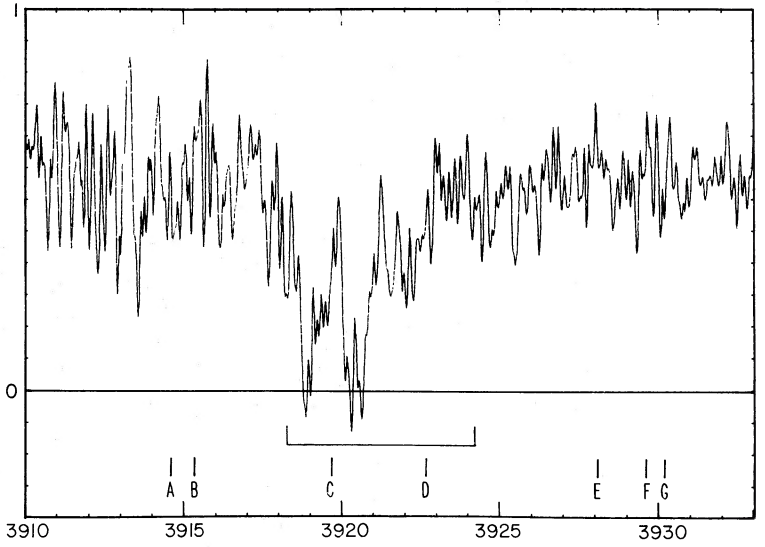

FIG. 2

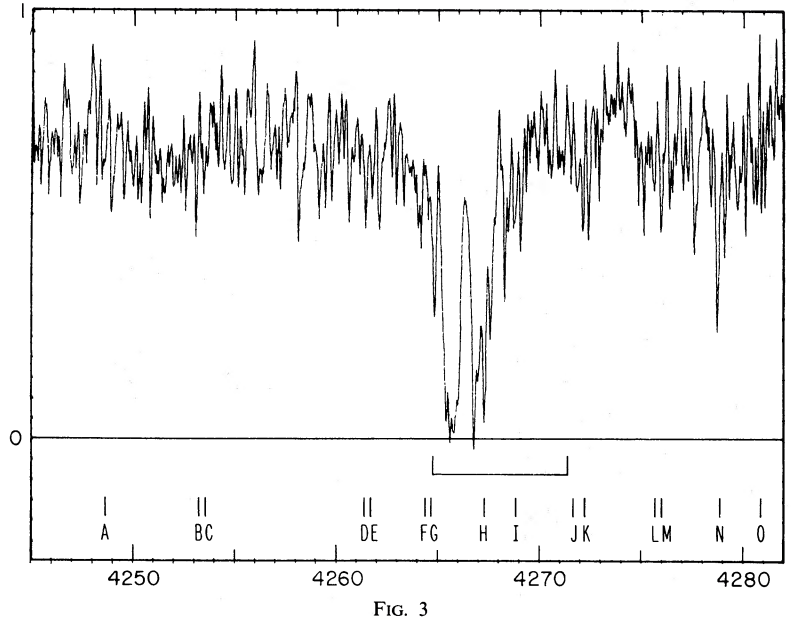

FIG. 3

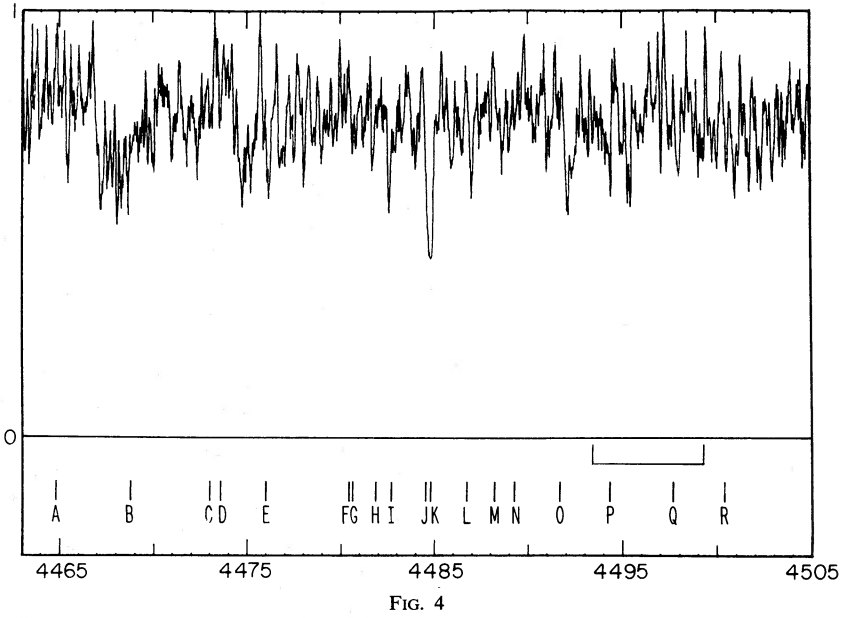

FIG. 4

FIG. 1.—MMT echelle spectrum of Si IV λ1393. Lettered lines indicate predicted positions of metal lines from other redshift systems.
FIG. 2.—MMT echelle spectrum of Si IV λ1403. Lettered lines indicate predicted positions of metal lines from other redshift systems.
FIG. 3.—MMT echelle spectrum of Si II λ1526. Lettered lines indicate predicted positions of metal lines from other redshift systems.
FIG. 4.—MMT echelle spectrum of Fe II λ1608. Lettered lines indicate predicted positions of metal lines from other redshift systems.

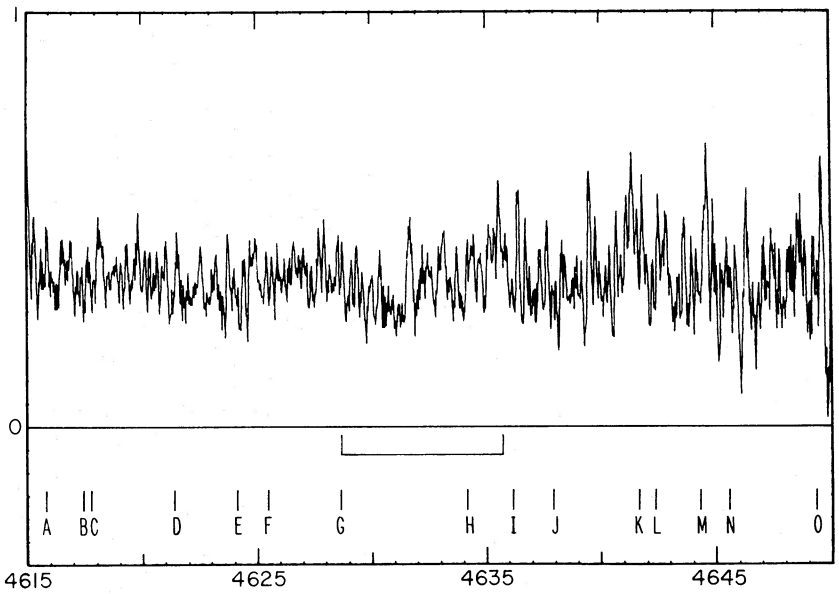

FIG. 5

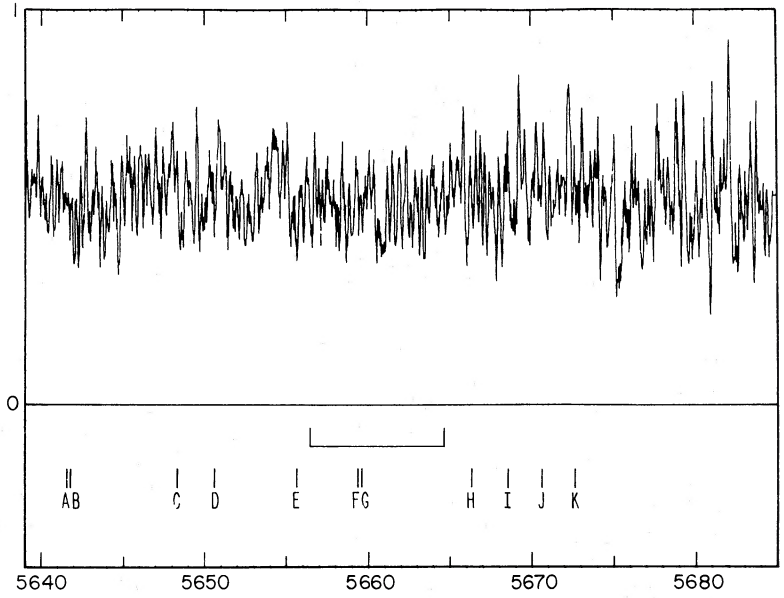

FIG. 6

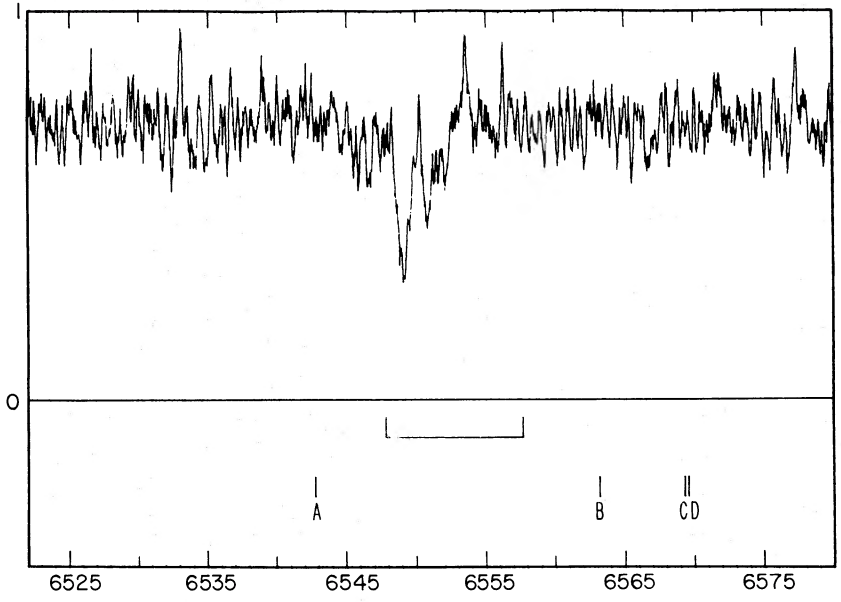

FIG. 7

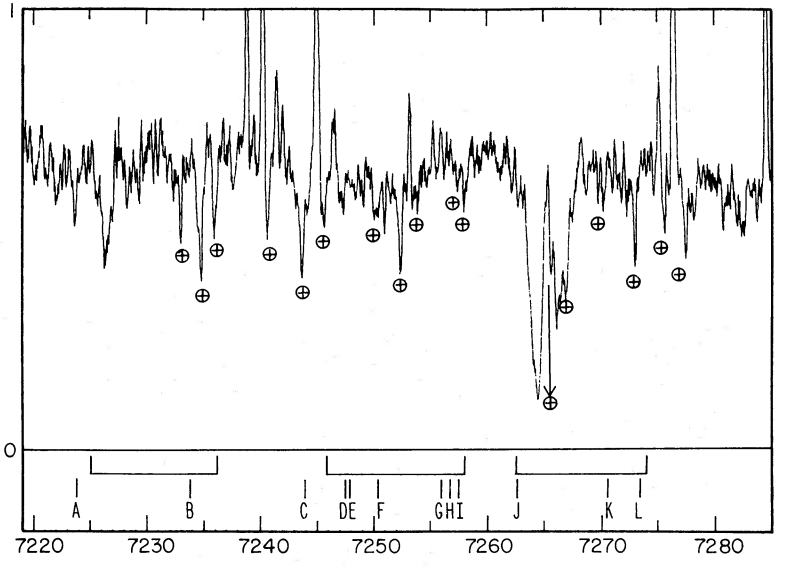

FIG. 8

FIG. 5.—MMT echelle spectrum of C I λ1657. Lettered lines indicate predicted positions of metal lines from other redshift systems.

FIG. 6.—MMT echelle spectrum of Zn II λ2025. Lettered lines indicate predicted positions of metal lines from other redshift systems.

FIG. 7.—MMT echelle spectrum of Fe II λ2344. Lettered lines indicate predicted positions of metal lines from other redshift systems.

FIG. 8.—MMT echelle spectrum of Fe II λλ2600, 2586, and Mn II λ2594. Lettered lines indicate predicted positions of metal lines from other redshift systems. The symbol ⊕ marks the positions of telluric absorption lines.

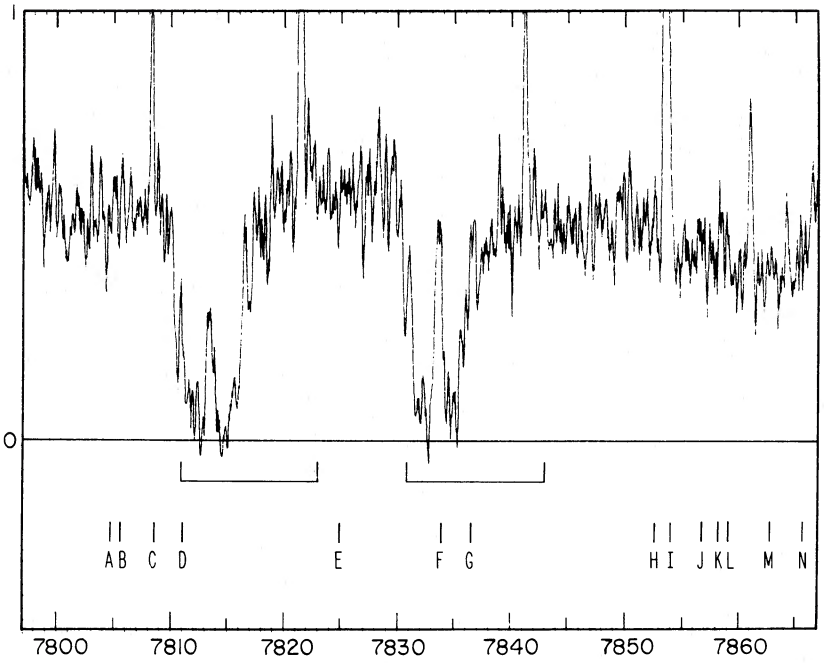

FIG. 9.—MMT echelle spectrum of Mg II λλ2796 and 2803. Lettered lines indicate predicted positions of metal lines from other redshift systems.

ponent. The profiles of the Fe II lines were fitted first, and the redshifts of the Fe II velocity components were used as a starting point for fitting the Mg II and Si II profiles. The *f*-value of the λ1608 transition of Fe II was regarded as uncertain, so that its profile was not used to derive component parameters. Instead, the column densities and *b*-values predicted from the other Fe II lines were used to predict the λ1608 profile which turned out to be consistent with the data for the *f*-value listed in Table 3.

In all cases, the line profiles were decomposed into the minimum number of components required to achieve an acceptable fit. Additional components (with smaller column densities and/or Doppler widths) can be added, but are not necessary. The inherent arbitrariness in the fitting procedure for these complex, blended profiles results in uncertainty in the specific properties of individual velocity components. It is noteworthy, in fact, that at 10 km s^{-1} resolution, few of the observed line profiles are consistent with simple, single-temperature Voigt profiles. At higher resolution, it is likely that these lines would split further into distinct velocity components.

In addition, errors in the column densities and Doppler

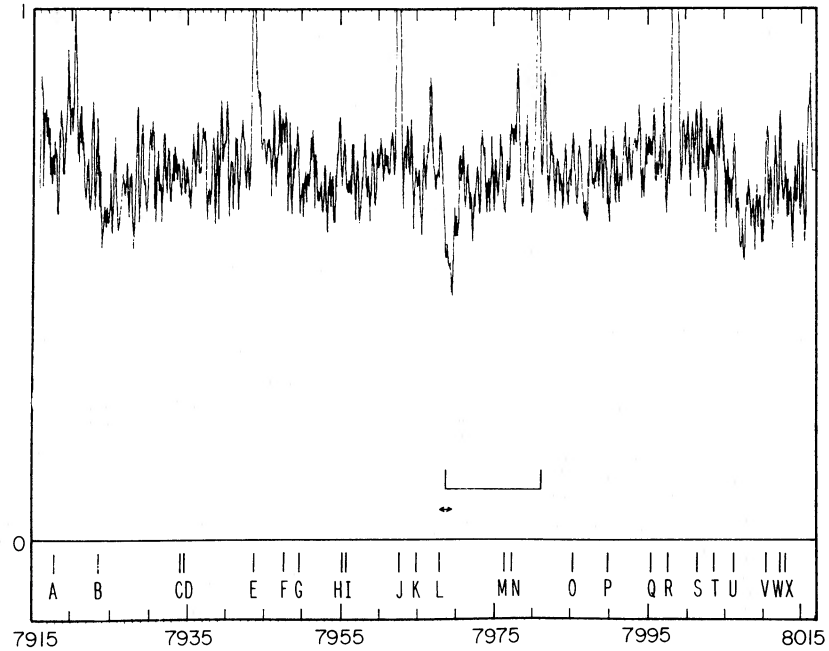

FIG. 10.—MMT echelle spectrum of Mg I λ2852. Lettered lines indicate predicted positions of metal lines from other redshift systems.

TABLE 2

OTHER POSSIBLE LINES FROM OTHER SYSTEMS

Line	Label	λ	Transition	Z
Si IV λ1393.....	A	3879.31	C II(1334)	1.90745
	B	3890.54	Si IV(1393)	1.79197
	C	3890.78	C II(1334)	1.91605
	D	3906.38	Si IV(1393)	1.80333
Si IV λ1403.....	A	3914.60	Si IV(1393)	1.80960
	B	3915.19	Si IV(1403)	1.79197
	C	3919.71	C II(1334)	1.93812
	D	3922.70	C II(1334)	1.94035
	E	3928.01	Si IV(1393)	1.81923
	F	3929.73	Si IV(1393)	1.82046
	G	3931.13	Si IV(1403)	1.80333
Si II λ1526	A	4248.58	Si IV(1403)	2.02940
	B	4253.09	C II(1334)	2.18768
	C	4253.40	Si IV(1394)	2.05245
	D	4261.55	Si II(1526)	1.79197
	E	4261.73	Si IV(1394)	2.05843
	F	4264.32	C II(1334)	2.19610
	G	4264.76	C IV(1548)	1.75528
	H	4267.24	Si IV(1403)	2.04270
	I	4268.90	C IV(1548)	1.75795
	J	4271.84	C IV(1550)	1.75528
	K	4272.09	Si IV(1403)	2.04616
	L	4275.84	C IV(1548)	1.76244
	M	4275.99	C IV(1550)	1.75795
	N	4278.90	Si II(1526)	1.80333
	O	4280.91	Si IV(1403)	2.05245
Fe II λ1608.....	A	4464.64	C IV(1550)	1.87962
	B	4468.52	C IV(1548)	1.88691
	C	4472.78	C IV(1548)	1.88967
	D	4473.41	Al II(1670)	1.67803
	E	4475.94	C IV(1550)	1.88691
	F	4480.21	C IV(1550)	1.88967
	G	4480.30	Si IV(1394)	2.21527
	H	4481.66	C IV(1548)	1.89540
	I	4482.38	Si IV(1403)	2.19610
	J	4484.43	C IV(1548)	1.89719
	K	4484.63	Si II(1526)	1.93812
	L	4486.82	C IV(1548)	1.89874
	M	4488.06	Si II(1526)	1.94035
	N	4489.10	C IV(1550)	1.89540
	O	4491.88	C IV(1550)	1.89719
	P	4494.28	C IV(1550)	1.89874
	Q	4497.69	C IV(1548)	1.90576
	R	4500.31	C IV(1548)	1.90745
C I λ1657	A	4615.45	C IV(1550)	1.97689
	B	4617.12	Si II(1526)	2.02491
	C	4617.60	C IV(1548)	1.98323
	D	4621.15	C IV(1550)	1.98057
	E	4623.97	Si II(1526)	2.02940
	F	4625.27	C IV(1550)	1.98323
	G	4628.42	C IV(1548)	1.99022
	H	4634.02	C IV(1548)	1.99384
	I	4636.11	C IV(1548)	1.99022
	J	4637.96	C IV(1548)	1.99638
	K	4641.72	C IV(1550)	1.99384
	L	4642.34	C IV(1548)	1.99921
	M	4644.27	Si II(1526)	2.04270
	N	4645.66	C IV(1550)	1.99638
	O	4649.55	Si II(1526)	2.04616
Zn II λ2025	A	5641.41	Al III(1862)	2.02940
	B	5641.61	Al III(1854)	2.04270
	C	5648.02	Al III(1854)	2.04616
	D	5650.33	Si II(1808)	2.12361
	E	5655.45	Si II(1808)	2.12897
	F	5659.68	Al III(1854)	2.05245
	G	5659.70	Si II(1808)	2.13133
	H	5666.18	Al III(1862)	2.04270
	I	5668.65	Si II(1808)	2.13628
	J	5670.78	Al III(1854)	2.05843
	K	5672.61	Al III(1862)	2.04616
Fe II λ2344	A	6542.85	Fe II(2344)	1.79197
	B	6563.05	Fe II(2382)	1.75528
	C	6569.42	Fe II(2382)	1.75795
	D	6569.49	Fe II(2344)	1.80333
Fe II λ2600	A	7223.57	Fe II(2344)	2.08245
	B	7233.65	Fe II(2344)	2.08675
	C	7243.91	Fe II(2344)	2.09113
	D	7247.24	Fe II(2344)	2.09255
	E	7247.68	Fe II(2382)	2.04270
	F	7250.42	Fe II(2344)	2.09391
	G	7255.90	Fe II(2382)	2.04616
	H	7256.70	Fe II(2344)	2.09659
	I	7257.23	Fe II(2600)	1.79197
	J	7262.66	Fe II(2344)	2.09913
	K	7270.90	Fe II(2382)	2.05245
	L	7273.48	Fe II(2344)	2.10375
Mg II	A	7804.79	Mg II(2796)	1.79197
	B	7805.65	Mg I(2852)	1.73687
	C	7808.35	Mg I(2852)	1.73782
	D	7810.96	Fe II(2600)	2.00499
	E	7824.81	Mg II(2803)	1.79197
	F	7833.68	Fe II(2600)	2.01374
	G	7836.56	Mg II(2797)	1.80332
	H	7852.27	Fe II(2600)	2.02089
	I	7854.08	Mg II(2797)	1.80960
	J	7856.68	Mg II(2803)	1.80333
	K	7858.16	Mg I(2852)	1.75528
	L	7858.94	Fe II(2600)	2.02345
	M	7862.73	Fe II(2600)	2.02491
	N	7865.78	Mg I(2852)	1.75795
Mg I	A	7917.97	Fe II(2600)	2.04616
	B	7923.34	Mg II(2797)	1.83437
	C	7934.34	Fe II(2600)	2.05245
	D	7934.68	Mg II(2797)	1.83843
	E	7943.68	Mg II(2803)	1.83437
	F	7947.47	Mg II(2797)	1.84300
	G	7949.88	Fe II(2600)	2.05843
	H	7955.05	Mg II(2803)	1.83843
	I	7955.72	Mg II(2797)	1.84595
	J	7962.82	Mg I(2852)	1.79197
	K	7964.94	Mg II(2797)	1.84925
	L	7967.87	Mg II(2803)	1.84300
	M	7976.15	Mg II(2803)	1.84595
	N	7977.25	Mg II(2797)	1.85365
	O	7985.39	Mg II(2803)	1.84925
	P	7989.94	Mg II(2796)	1.85819
	Q	7995.23	Mg I(2852)	1.80333
	R	7977.72	Mg II(2803)	1.85365
	S	8001.57	Mg II(2796)	1.86236
	T	8003.93	Fe II(2600)	2.07922
	U	8006.24	Fe II(2600)	2.08011
	V	8010.45	Mg II(2803)	1.85819
	W	8013.11	Mg I(2852)	1.80960
	X	8012.31	Fe II(2600)	2.08245

TABLE 3

ATOMIC CONSTANTS

Species	λ(vac)	f	Γ/10⁸	Reference
Si II	1526.709	0.230	6.50	1
Fe II	1608.456	0.0963	2.60	2
C I	1656.928	0.136	3.30	3
Zn II	2026.059	0.412	3.35	3
Mg I	2026.477	0.110	0.96	4
Fe II	2344.213	0.108	2.40	5
	2586.650	0.0573	2.60	5
Mn II	2594.508	0.223	2.21	3
Fe II	2600.172	0.203	2.60	4
Mg II	2796.352	0.592	2.51	3
	2803.530	0.295	2.53	3
Mg I	2852.965	1.770	5.20	4

REFERENCES.—(1) Shull, Snow, and York 1981; (2) Nussbaumer, Pettini, and Storey 1982; (3) Morton and Smith 1973; (4) Morton 1978; (5) Lugger *et al.* 1982.

parameters result from photon noise, systematic uncertainty in the zero point (discussed above), and scattered light. We estimate that the uncertainties from these effects result in errors of about 50% in column densities for the unsaturated lines. Many of the velocity components have lines which are heavily saturated. For these components, only lower limits to the column densities can be derived.

IV. DISCUSSION

a) *Line Profiles*

In Figures 11*a* and 11*b*, we plot line profiles on a velocity scale for Mg I λ2852, Mg II λ2796 and λ2803, Fe II λ2343 and λ2600, Si II λ1526, C IV λ1548 and λ1550, and Si IV λ1393 and λ1403. The zero velocity was arbitrarily chosen to be the center of the strongest observed feature of Fe II in the profile, $z = 1.794671$. The center of the Mg I profile, whose absolute redshift is uncertain by 13 km s^{-1} for reasons described above, was shifted by +8 km s^{-1} in order to be centered at zero velocity.

While the decomposition of these profiles into Voigt components is arbitrary, it is however clear from Figures 11*a* and 11*b* that the absorption profiles differ significantly from species to species. Material with velocity near 0 km s^{-1} absorbs strongly in all transitions, with Si IV weaker than C IV, and Si II stronger than Si IV. Material at a relative velocity of −50 km s^{-1} has very weak Mg I or Fe II absorption, Si IV stronger than Si II, and intermediate-strength C IV and Mg II. At a velocity of +50 km s^{-1}, Si IV is stronger than C IV, Mg II and Si II are strong, Fe II weak, and Mg I absent. Toward positive relative velocities, Si II and Mg II decrease in strength and become undetectable for $v > +200$ km s^{-1}; C IV also becomes weaker but is detectable to $v = +450$ km s^{-1}.

Our data appear to favor the interpretation that this system is a single galaxy with a halo of greater velocity dispersion than our own, rather than the superposition of absorption arising in the overlapping halos of several galaxies in a cluster (see, e.g., Pettini *et al.* 1983; Paper I). The low-ionization species (Mg II, Fe II, Si II, and Mg I) show velocity structure which is similar to the structure seen in the same species in lines of sight through the Milky Way (e.g., Cohn and York 1977; Savage and de Boer 1979). Only C IV and Si IV show the unusually large velocity spread seen in some quasar systems, and not seen in our Galaxy. Unlike some of the complex quasar systems, however (see, e.g., Blades *et al.* 1982; Pettini *et al.* 1983), the strength of

TABLE 4A

$Z = 1.79$ LINE LIST: Si II

Transition	λ(obs)	z	EW (mÅ)	b (km s^{-1})
Si II λ1526	4264.82	1.794093	114	<3
	4265.67	1.794651	917	<17
	4266.77	1.795371	331	<5
	4267.00	1.795522	129	<5
	4267.25	1.795685	234	<4
	4267.58	1.795900	153	<5
	4268.28	1.796361	110	<3.4

TABLE 4B

$Z = 1.79$ LINE LIST: Fe II

	λ(obs)	z	EW (mÅ)	b (km s^{-1})	τ	N (cm^{-2})
1.....	6547.84	1.794093	<54	...	<1.1	5 E12
	7224.98		<38		<0.64	
	7262.76		<88		<2.3	
	4493.17					
2.....	6548.60	1.794415	66	<3	0.93	6 E12
	7225.82		47		0.55	
	7263.59		115		1.94	
	4493.69					
3.....	6548.87	1.794531	120	3.2	1.47	1.2 E13
	7226.12		90		0.86	
	7263.94		188		3.06	
	4493.87					
4.....	6549.20	1.794671	205	6.7	1.14	2 E13
	7226.48		153		0.66	
	7264.27		348		2.37	
	4494.10					
5.....	6549.58	1.794834	129	<6	0.68	1.1 E13
	7226.90		91		0.40	
	7264.68		242		1.43	
	4494.36					
6.....	6550.03	1.795026	40	<4	0.27	3 E12
	7227.40		27		0.16	
	7265.18		84		0.56	
	4494.67					
7.....	6550.81	1.795358	105	<5	0.72	9 E12
	7228.26		74		0.42	
	7266.08		192		1.51	
	4495.20					
8.....	6551.07	1.795469	67	<4	0.60	5.5 E12
	7228.54		47		0.35	
	7266.34		126		1.26	
	4495.38					
9.....	6551.36	1.795593	63	<4	0.49	5.0 E13
	7229.09		43		0.29	
	7266.66		122		1.02	
	4495.58					
10.....	6551.64	1.795713	52	<4	0.39	4.0 E13
	7229.40		43		0.29	
	7266.97		105		0.82	
	4495.77					
11.....	6552.13	1.795922	40	<4	0.33	3.0 E12
	7229.94		27		0.19	
	7267.51		82		0.69	
	4496.11					
12.....	6553.05	1.796314	<25	...	<0.44	<2 E12
	7230.96		<17		<0.26	
	7268.53		<51		<0.92	
	4496.74					

TABLE 4C

$Z = 1.79$ LINE LIST: Mg II

	λ(obs) (Å)	z	EW (mÅ)	b (km s^{-1})	τ	N (cm^{-2})
1.....	7810.61	1.794059	323	<4.5	4.4	
	7830.67		242		2.2	
2.....	7811.40	1.794362	564	<8.2	3.9	
	7831.52		422		1.9	
3.....	7812.05	1.794551	641	<8.2	6.0	
	7832.05		512		3.0	
4.....	7812.75	1.794808	779	<6.4	sat	
	7832.77		724		sat	
5.....	7813.70	1.795219	257	5.8	1.5	3.5 E12
	7833.92		157		0.74	
6.....	7814.20	1.795358	446	<5.2	5.0	
	7834.31		382		2.5	
7.....	7814.72	1.795526	558	<5.2	sat	
	7834.78		510		sat	
8.....	7815.17	1.795704	526	<5.2	sat	
	7835.28		470		sat	
9.....	7815.89	1.795918	473	<5.2	sat	
	7835.88		405		sat	
10.....	7817.00	1.796328	209	4.5	1.64	3.0 E12
	7837.03		132		0.82	

TABLE 4D

$Z = 1.79$ LINE LIST: OTHER SPECIES

Species	λ(obs) (Å)	Z	EW (mÅ)	τ	N (cm^{-2})
Mg I λ2852.....	7969.22	1.794216	255	0.33	8.0 E11
C I λ1656.....	4631	...	<142	...	<2 E13
Zn II λ2025.....	5659	...	<78	...	<2.5 E12
Mn II λ2594.....	7254	...	<50	...	<3.8 E12
Mg I λ2025.....	5659	...	<78	...	<2 E13

the C IV absorption is a smoothly changing function of velocity, suggesting organized motion in the halo of a single galaxy.

The Si II/Si IV ratio, which is greater than one at zero velocity, but less than one at $v > +130$ km s^{-1}, suggests that the ionization varies with velocity. Thus, the components at $v > 200$ km s^{-1} are weak in Mg II and Si II not only because the column densities of all species are lower, but also because the ionization is higher.

The asymmetry of the C IV profile and the trend of ionization and column density with velocity can be naturally explained if our line of sight to B2 1225+317 is passing through a rotating ensemble of clouds (Weisheit 1978) and the ionization within each cloud increases with radius from the center of the ensemble. For example, one might imagine this system to be the photoionized gaseous halo of a galaxy corotating with its disk, with the mean density of the gas decreasing with radius. Other simple models such as an ensemble of clouds uniformly expanding or uniformly infalling will generally give symmetric aggregate profiles. In the particular case of this system in B2 1225+317, the profile asymmetry toward positive velocity implies rotation toward us. The rather large velocity width of the aggregate profile argues against this picture, however. There are other ways to produce asymmetric profiles such as the picture discussed by York *et al.* (1986) where the absorption arises in the halo of a large galaxy and the gas of its associated Magellanic-type irregulars. In this case, the large velocity width results from mechanical motions induced by supernovae.

A further unfortunate consequence of the single rotating halo model is that there is no unique correspondence of velocity with position in the galaxy. Absorption at $v = +200$ km s^{-1}, for example, arises from material located at opposite sides of the halo. Since it would be fortutious if the physical conditions of the gas at these two places were the same, the interpretation of line ratios in terms of physical parameters is ambiguous.

The comparison of statistical results from surveys of absorbers discovered in different ways has led several authors to postulate multiphase models for the origin of the metal-line systems. Certainly our observations support these ideas. Early searches for C IV and Mg II doublets (Weymann *et al.* 1979; Young *et al.* 1982) suggested that the mean free path for absorption by C IV was smaller than that for Mg II, but the errors are large, and the redshift range for which homogeneous data exist for C IV ($1.1 < z < 2.3$) did not overlap with that of Mg II ($0.16 < z < 0.83$). Lyman discontinuities, for which data existed in the redshift range $0.37 < z < 3.5$, have mean free paths for absorption which are consistent with those of both C IV and Mg II. These thick Lyman-limit systems almost always have detectable Mg II or C IV absorption, although C IV absorbers do not always have associated Lyman edges (Betchtold *et al.* 1984). C IV is often stronger than the C II (Wolfe 1983), Mg II, or Fe II (Bergeron and Boisse 1984) absorption, with a tendency for the systems which show only C IV to have low equivalent widths and be optically thin at the Lyman limit.

Roughly speaking, one can divide the narrow, metal-line systems into at least two groups, based on their observable properties: (1) those which are optically thick in the Lyman limit, show Mg II and C IV and sometimes 21 cm in absorption (Briggs and Wolfe 1983), and probably do not evolve with z, and (2) those which are thin at the Lyman limit, show C IV but no C II or Mg II, and may show some mild evolution with z (Bergeron and Boisse 1984). The interpretation of the first type of system as arising in an intervening galaxy is relatively uncontroversial. The second type, whose properties are so different from the properties of material seen in absorption in our galactic ISM or halo, is perhaps less easily identified with an intervening galaxy. Chaffee *et al.* (1986) and Paper II argue that the physical conditions and/or metal abundance of these C IV absorbers are very different from the Lyman-α forest absorbers, but an origin in ejecta from an intervening QSO may be suggested (Briggs, Turnshek, and Wolfe 1984; Hazard 1984, private communication). However, the existence of C IV absorbers with no corresponding Mg II or C II (Paper II) in the $z = 1.79$ system in B2 1225+317 argues that the optically thin, low column density C IV absorbers with C IV > C II can be associated with galaxies. Perhaps the other examples of these systems arise in lines of sight passing through the outermost regions of galactic halos, at an impact parameter larger than that in the $z = 1.79$ system discussed here. One objection to this conclusion might be the estimated sizes of the C IV system at $z = 2.12$ also seen toward B2 1225+317 (Paper II and Chaffee *et al.* 1986); photoionization models imply a diameter of about 6 kpc for that cloud. This size estimate depends on the ultraviolet photon field, assumed to be the integrated QSO background, which is uncertain, but if 6 kpc is indicative of typical cloud dimensions, it is hard to imagine that more than a few such large clouds could exist in a single halo. On the other hand, local sources of ionizing photons could reduce the size of the clouds.

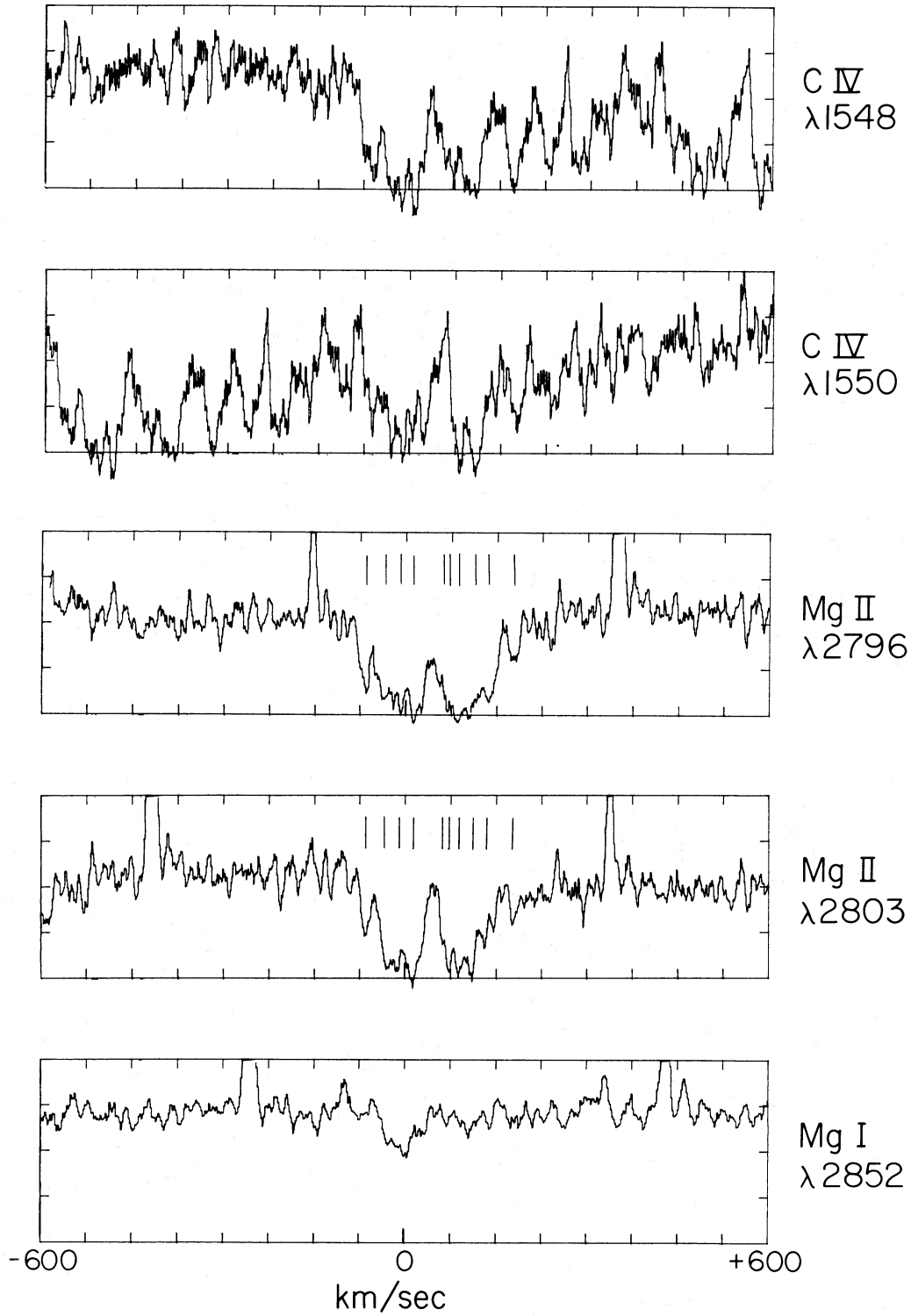

FIG. 11*a*.—$z = 1.79$ velocity profiles: C IV, Mg II, and Mg I. Vertical lines indicate position of components listed in Table 4.

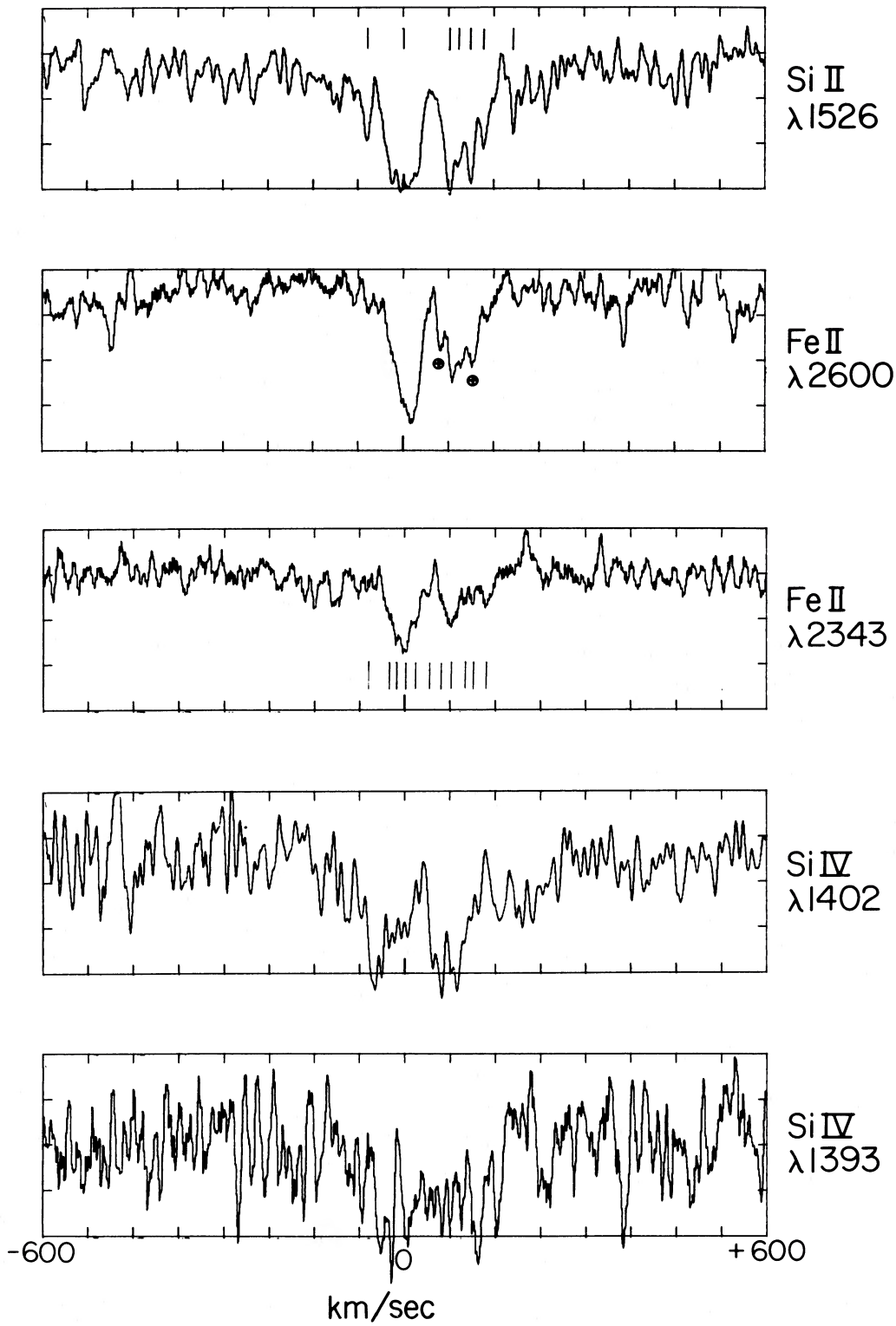

FIG. 11*b*.—$z = 1.79$ velocity profiles: Si IV, Fe II, and S II. Vertical lines indicate position of components listed in Table 4.

b) Element Abundances: Fe II *and the Search for* Zn II

One of the goals of this study is to measure the abundances of elements relative to hydrogen and compare them to the abundances observed in the interstellar medium (ISM) of our Galaxy. A large body of data exists for the Milky Way ISM from the *Copernicus* satellite (Bohlin *et al.* 1983), and relative abundances for several elements have recently been derived (Jenkins, Savage, and Spitzer 1985). In addition, gas in the Milky Way halo has been studied by observing halo stars (Pettini and West 1982) and stars in the LMC and SMC (Savage and deBoer 1979, 1981; Fitzpatrick 1984, and references therein) with *IUE*.

There are several sources of uncertainty which affect the derivation of abundances from absorption-line studies. First, the column density of hydrogen and of the heavy element species must be measured. In practice, this is difficult because lines strong enough to be detected are often saturated. Second, the columns of several ionization states must be measured for each element, or some correction made for ionization in the context of a model. Third, the gas phase abundance of elements in the interstellar medium suffers depletion by dust grains, which can change apparent metal-to-hydrogen ratios by factors of up to 1000 in the case of calcium and 100 in the case of Fe II.

The determination of N(H I) in the $z = 1.79$ system in B2 1225+317 is more difficult than the determination of N(H I) for the typical ISM line of sight studied by *Copernicus*. All of the lines of sight studied with *Copernicus* in Lyman-α by Bohlin, Savage, and Drake (1978) have log N(H I) > 19.5 cm^{-2}, so that Lyman-α is on the damped part of the curve of growth, and N(H I) is quite well-determined from the line profile. By contrast, Lyman-α in the B2 1225+317 system is saturated but not evidently damped (Paper II). One must assume a reasonable b-value or reasonable set of b-values for blended velocity components, in order to determine column densities. Also, a damped component, say at "zero" velocity, could be hidden by narrow Lyman-α components in its wings, which make the profile appear "square." In Paper II we estimate that such a component must have N(H I) $< 5 \times 10^{18}$ cm^{-2} for any $b < 50$ km s^{-1}, or else the damping wings would have been seen. A lower limit on the total N(H I) summed for all velocity components is given by the observation of the Lyman limit with *IUE* (Snijders, Pettini, and Boksenberg 1981) which implies that the optical depth τ(LL) > 4 so that N(H I) $> 7 \times 10^{17}$ cm^{-2}; individual components, of course, are expected to have a value of N(H I) which is some fraction of the total. A less stringent lower limit on N(H I) can be placed for each component by noting that the observed Lyman-α line is black at the center; this lower limit on N(H I) depends on the b-value adopted. Assuming $b = 24$ km s^{-1}, N(H I) $> 3 \times 10^{14}$ cm^{-2}. At any rate, for this system, which has a relatively high column density for a typical QSO metal-line system, we estimate that N(H I) is at least a factor of 10 lower than the lowest column density line of sight studied by Bohlin, Savage, and Drake (1978). By contrast, the column density for Fe II, Si II, and Mg II are typical of components in unreddened lines of sight (York and Kinahan 1979).

One way to get around both the problems of heavy element depletion and of line saturation of Lyman-α is to measure the column density of Zn II. York and Jura (1982) and Harris, Bromage, and Blades (1983) have shown that zinc is undepleted by dust and hence is a reliable tracer of metallicity in the ISM. They showed that for H I regions, and 5×10^{19} cm^{-2} < N(H I) < 5×10^{21} cm^{-2}, log N(Zn II) = 1.02 × log N(H I) − 8.0, with a scatter in the relation of about 0.4 in the log. In standard nucleosynthesis scenarios, the zinc abundance relative to hydrogen is expected to vary directly with the iron abundance (Pagel 1986). Unfortunately, applying the N(Zn II)–N(H I) relation to B2 1225+317, with the most optimistic value for N(H I) = 5×10^{18} cm^{-2} [noting that this value lies outside the range of N(H I) of the ISM relation], we expect N(Zn II) = 1.2×10^{11} cm^{-2}, or for the λ2025 line, an observed equivalent width of 5 mÅ. The observed limit N(Zn II) < 2×10^{12} cm^{-2} implies N(Zn II)/N(H I) < 4×10^{-7} for N(H I) = 5×10^{18} cm^{-2}, compared to the solar value of N(Zn)/N(H) = $4 \pm 0.8 \times 10^{-8}$ (Biemont and Godefroid 1980). We can, however, infer that the total N(H I) + N(H II) < 5×10^{19} cm^{-2} for all components appearing in Fe II, if N(Zn)/N(H) is solar, and if the ionization is similar to that in neutral galactic clouds.

Determining the column densities of the other heavy elements is also difficult since for low column density lines of sight, weak and unsaturated lines are hard to detect. Ideally, for each species one would measure lines which have a range of f-values and construct a curve of growth. Often, in practice, a curve of growth is constructed for one or two species and then the derived b-values are adopted for other species in order to determine column densities from saturated lines. Unfortunately, for the B2 1225+317 system the complex nature of the line profile and the observed range of ionization means that the validity of this last procedure is questionable.

Fe II is the only species for which we have observations of lines on both the linear and flat part of the curve of growth. The column densities and b-values of individual velocity components are listed in Table 4. We note that with 10 km s^{-1} resolution, the typical upper limit to the Doppler width is somewhat higher than the temperature at which Fe II is the dominant form of iron, i.e., 15,000 K or 2.2 km s^{-1} (Shull and Van Steenberg 1983). This suggests that velocity substructure on smaller scales is probably present, and the column densities are correspondingly uncertain.

The classical way to distinguish between turbulent broadening by an ensemble of clouds with velocity dispersion v_t, and thermal broadening by a Maxwellian distribution of atoms at temperature, T, is to compare line widths of species with different atomic weights, m, but smaller ionization, since the observed width, b, is

$$b^2 = v_t^2 + kT/m \,. \quad (1)$$

The observed widths of the blended component centered at $v = 0$ (full width at half-maximum or 1.66 times the Doppler width b) are 70 km s^{-1}, 62 km s^{-1}, and 52 km s^{-1} for Mg II, Si II, and Fe II, respectively (which have $m = 24$, 28, and 56). Clearly, however, the naive application of equation (1) is not valid, since, if purely thermal (as implied by these ratios), the widths imply temperatures in excess of 10^6 K. It is possible that different subcomponents have different Mg II/Fe II and Si II/Fe II. For example, for collisional ionization equilibrium (Shull and Van Steenberg 1982), Mg II/Fe II varies by a factor of 4 for temperatures at which Mg II is within a factor of 10 of its peak ionization fraction. The ratio Si II/Fe II varies by a factor of 100 for temperatures at which Si II is within a factor of 10 of its peak. However, in the local ISM, these ratios are determined by photoionization by starlight so that they are expected to be almost independent of temperature. In addition, the different

f-values of the transitions we observed result in different sensitivities for the different lines.

Nevertheless, since the b-values of the Fe II components listed in Table 4 are only a factor of 2–3 larger than the predicted thermal widths for collisional equilibrium, we expect that there are only a few subclouds per component. Blindly associating the Fe II at $v = 0$ with the limits placed on N(H I) discussed above, we find that $-4.5 < \log [N(\text{Fe II})/N(\text{H I})] < -5.4$ compared to $\log [N(\text{Fe II})/N(\text{H})] = -5.85$ (with a scatter of about 0.2), from the *Copernicus* data (Jenkins, Savage, and Spitzer 1985). Given the caveats described above, the Fe/H ratio is consistent with what is observed in the interstellar medium of the Milky Way. The possible overabundance of Fe II in the QSO system can be accounted for if a large fraction of the Fe II containing gas is H II, as seems likely from the presence of several ionization stages, not H I. The resulting [Fe/H] < -5.4 then corresponds to depleted iron.

Similarly, the N(Mg II)/N(H) ratio can be compared to the ISM value. The lack of detection of Mg II $\lambda\lambda$1239, 1240 implies $N(\text{Mg II}) < 3 \times 10^{15}$ cm^{-2} (Paper II), and the saturation of Mg II $\lambda\lambda$2796, 2803 implies $N(\text{Mg II}) > 3 \times 10^{14}$ cm^{-2} per component. Thus, $-4.2 < \log [N(\text{Mg II})/N(\text{H I})] < -2.4$, compared to the interstellar $\log [N(\text{Mg II})/N(\text{H I})] = -4.70$ (with a scatter of 0.25) from *Copernicus* (Jenkins, Savage, and Spitzer 1985). Again, the Mg/H ratio is consistent with the ISM values.

The derived ratios of ions are $0.90 < \log [N(\text{Fe II})/N(\text{Zn II})]$ and $\log [N(\text{Fe II})/N(\text{Mg II})] = -1.18$. These ratios, which are fairly independent of ionization, are consistent with the abundances in the local ISM. In particular, both ratios are consistent with a gas where iron is already depleted by grain formation ([Fe/Mg]$_\odot \sim 1$).

c) Mg I/Mg II, C I/C II *and the Radiation Field Above the Lyman Limit*

Mg I and C I probe the neutral gas in this system. In the ISM, the C I produced in H II regions is negligible; C I is detected in absorption only in H I regions, where $T < 10^4$ K and shielding of ionizing photons by dust is probably important (Jenkins and Shaya 1979). For magnesium, a high dielectronic recombination coefficient at relatively low temperatures enhances the formation of Mg I. This, along with the high f-value of the Mg I λ2852 transition, means that Mg I is detectable in warm gas ($T = 10^4$ K) where C I is not (York and Kinahan 1979).

We placed a limit on C I for any velocity component of $N(\text{C I}) < 2 \times 10^{13}$ cm^{-2}. Unfortunately, C II λ1334 is saturated (Paper II) so that N(C II) is uncertain. We estimate that for the component at zero velocity the requirement that no damping wings be observed for C II λ1334 implies that $N(\text{C II}) < 4 \times 10^{18}$ cm^{-2}. For $b = 8$ km s^{-1}, the requirement that the absorption line be dark at the center as observed implies $N(\text{C II}) > 5 \times 10^{15}$ cm^{-2}. Thus, C II/C I > 250, and ignoring photoionization for the moment, the collisional equilibrium temperature must be $T > 10^{4.6}$ K.

Fitting the Mg I profile with one Voigt component yields $N(\text{Mg I}) = 8 \times 10^{11}$ cm^{-2} with $b = 18$ km s^{-1}. Since $T = 10^4$ K implies a thermal width for magnesium of 2.5 km s^{-1}, several subcomponents are probably present, each with higher $N(\text{Mg I}) < 2 \times 10^{13}$ cm^{-2}. We take 8×10^{11} cm^{-2} as an upper limit to the N(Mg I) for each subcomponent. For the Mg II column, we estimate that at zero velocity, $N(\text{Mg II}) < 3 \times 10^{15}$ cm^{-2} from lack of observable $\lambda\lambda$1239, 1240 (Paper II), $N(\text{Mg II}) = 3 \times 10^{14}$ cm^{-2} from fitting $\lambda\lambda$2803, 2796, and $N(\text{Mg II}) = 2.8 \times 10^{14}$ cm^{-2} from the value of the Fe II column at zero velocity, assuming the ISM [Fe II/Mg II] ≈ -1.2 (Jenkins, Savage, and Spitzer 1985). Adopting $N(\text{Mg II}) = 3 \times 10^{14}$ cm^{-2} results in Mg II/Mg I > 350. This is similar to the observed ISM values of Mg II/Mg I > 500 (Bruhweiler *et al.* 1984) and $60 <$ Mg II/Mg I < 800 in the combined data of Pettini *et al.* (1977) and Murray *et al.* (1984). Again, ignoring photoionization, the collisional equilibrium temperatures implied are $T > 10^{4.7}$ K (with most of the magnesium in the form of Mg III), consistent with the temperatures implied by the C II/C I ratio. These calculations imply much greater total hydrogen columns N(H I) + N(H II) than N(H I), because at such high temperatures, H is highly ionized.

Since both Mg I and C I can be ionized by photons redward of the Lyman limit, they can, in principle, yield information about different sources of the local radiation field than species whose ionization potentials fall blueward of the Lyman limit. In the halo of a galaxy, for example, the radiation field for $\lambda > 912$ Å could be dominated by stellar light from the galaxy, or by the diffuse background from other normal galaxies (see, e.g., York 1982). Below 912 Å, most stellar light may be absorbed by disk H I, and the summed radiation from other sources, such as QSOs, might be expected to dominate.

We investigated these issues by constructing photoionization models using the code CLOUDY, lent to us by Gary Ferland (Ferland 1981; Ferland and Truran 1981). In Figures 12 and 13 we plot Mg I/Mg II and C I/C II as functions of ionization parameter, here defined as

$$U = \frac{Q(\text{H})}{4\pi r^2 cn},$$

under different assumptions for the ionizing field, where Q is the number of ionizing photons per second beyond the Lyman limit. The calculations are similar to those presented by Chaffee *et al.* (1986). It is assumed that the clouds are plane-parallel slabs illuminated on one face, at constant pressure. The models were calculated with solar metallicity, where the solar logarithmic abundances with respect to hydrogen were taken to be

$$\text{He:C:N:O:Mg:Si} = -1.0:-3.33:-4.01:-3.08:-4.59:-4.40\,.$$

The thermal structure of the cloud and ionization levels were found to be insensitive to the metallicity for the ionization parameters considered here. The equilibrium temperatures were consistent with the derived b-values for C IV and Mg II.

For energies between 1 and 16 rydbergs (912 Å–57 Å), we adopted the radiation field from the integrated contribution of QSOs at $z = 1.79$, as calculated by Bechtold *et al.* (1986*b*). As Bechtold *et al.* discuss, this radiation field is uncertain due to uncertainties in the QSO luminosity function (in particular, the assumed form at high redshifts), the adopted intrinsic spectrum of the QSOs in the far-UV, and the role of continuum absorption by intervening material. In the discussion below, we adopt an ionizing continuum with mean spectral slope between 1 and 16 rydbergs of -1.7, with $\log J_\nu = -21.84$ ergs cm^{-2} s^{-1} Hz^{-1} at 912 Å, and the total number of ionizing photons beyond the Lyman limit, $\log Q = 5.37$. The shape was taken to be that of the "medium" radiation field at $z = 1.79$, interpolated from the values given in Table 3 of Bechtold *et al.*

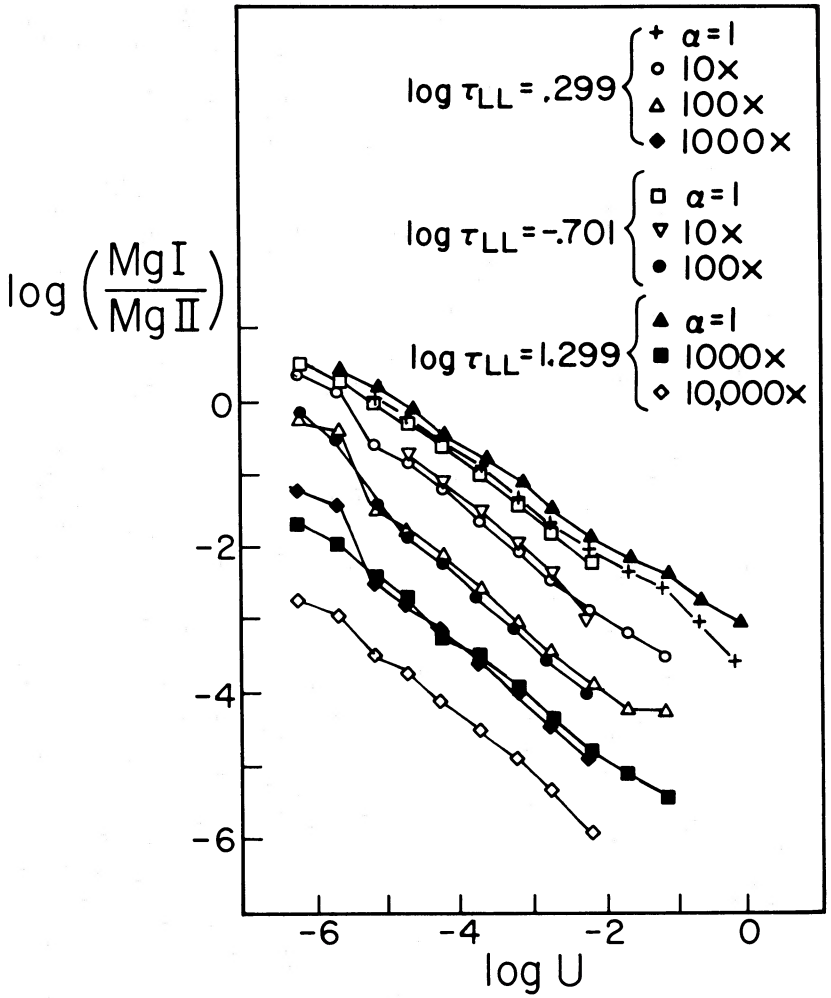

FIG. 12

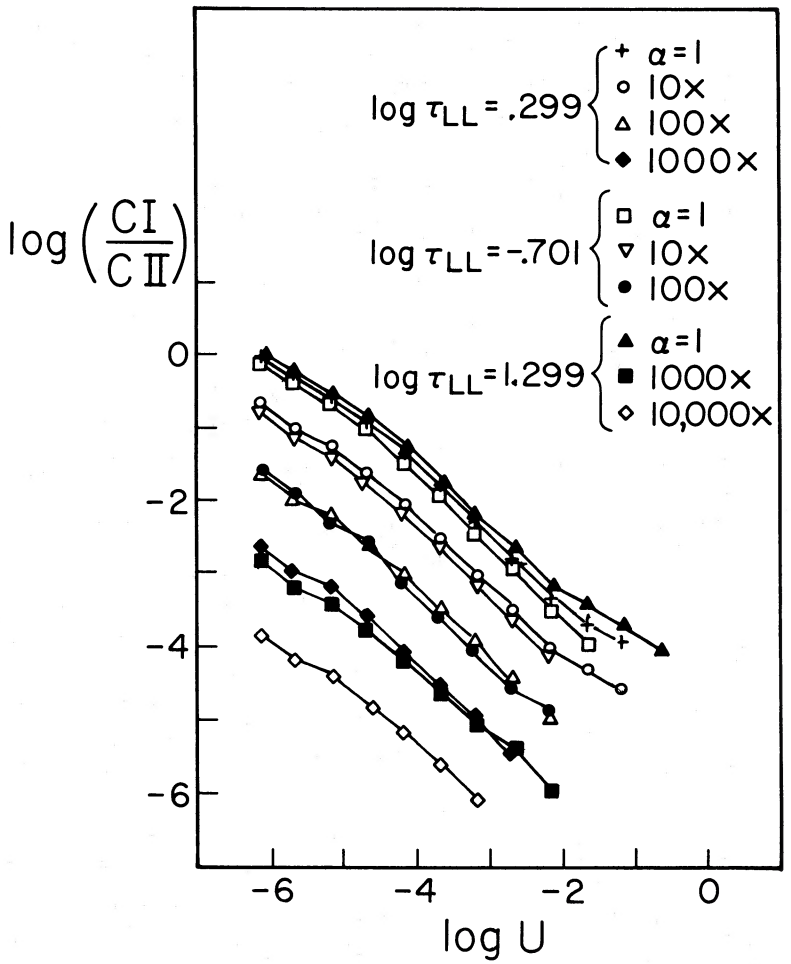

FIG. 13

FIG. 12.—The dependence of Mg I/Mg II on the radiation field
FIG. 13.—The dependence of C I/C II on the radiation field

(1986*a*). We estimate the uncertainty in this normalization to be about a factor of 10 at $z = 1.79$. The spectrum below 16 rydbergs was assumed to be a power law with spectral index 0.7. The results of the model calculations are completely insensitive to the shape of the X-ray spectrum below 40 keV. The ionization fractions are changed by about 10% for the optically thin models and 15% for the thick models when the spectral index softer than 40 keV is varied between 0.5 and 1.0.

The spectrum for wavelengths redward of 912 Å was varied in order to generate the results shown in Figures 12 and 13. The contribution by QSOs to the radiation longward of 912 Å is well-described by a power law of slope about 1.0. We then considered models with this slope, but with 10, 100, 10^3, and 10^4 times the normalization for $\lambda > 912$ Å. The thermal structure of the cloud and the distribution of ions whose ionization potentials are larger than 1 rydberg changed by less than 10% when the optical fluxes were varied. Models were run so that the total log N(H I) = 16.5, 17.5, and 18.5 cm^{-2} corresponding to optical depths at the Lyman limit of 0.2, 2.0, and 20, respectively. The ratios Mg I/Mg II and C I/C II are not sensitive to optical depth effects, for moderate optical depths. These ratios are apparently most sensitive to the flux longward of 912 Å.

The observed ionic ratios then depend on the ionization parameter, U, and the shape of the ionizing spectrum. In order to estimate the photon field, given observed line ratios and a shape, some estimate of n_e must be made. One way to measure n_e is to observe the population of the fine-structure excited states relative to their ground state (Bahcall and Wolf 1968). In Paper II, we set limits on the excited state of C II, C II* λ1335, with N(C II*) $< 3 \times 10^{13}$ cm^{-2} for the zero velocity component, and N(C II*) $< 1 \times 10^{13}$ cm^{-2} for all other components. At densities below the critical density where collisional de-excitation depletes the upper states, the upper levels are populated by collisions, by direct excitation by IR photons, or by excitation by UV photons to higher levels which subsequently decay to the ground-state fine-structure level. The most conservative upper limit to the density is then given by assuming collisional excitation only, in which case

$$\frac{n(\text{C II*})}{n(\text{C II})} = n_e(0.0263)\left(\frac{T}{10{,}000\ \text{K}}\right)^{-1/2} . \quad (2)$$

When more modern rate constants are used, the numerical coefficient on the right-hand side of this equation becomes 0.0341 (J. Black 1985, private communication). Adopting the conservative value N(C II) $= 5 \times 10^{15}$ cm^{-2}, and $T =$ 20,000 K, we estimate from equation (2) that $n_e < 0.51$ cm^{-3}.

For the normalization of the QSO field adopted above, this translates to a limit on the ionization parameter, log $U > -4.6$. From Figure 12 the observed log (Mg I/Mg II) $= -2.5$ implies that the specific intensity at 1000 Å, J_ν(1000 Å), is less than about 500 times the QSO field, log J_ν(1000 Å) < -19.1 ergs s^{-1} cm^{-2} Hz^{-1}. Similarly, for log (C I/C II) < -2.4, J_ν(1000 Å) is less than 100 times the QSO field, or log J_ν(1000 Å) < -19.8 ergs s^{-1} cm^{-2} Hz^{-1}. By comparison, the diffuse radiation field due to galactic sources is estimated to be log J_ν(1000 Å) $= -18.2$ ergs s^{-1} cm^{-2} Hz^{-1} in the solar neighborhood, decreasing as one moves out of the galactic plane to log J_ν(1000 Å) $= -19.9$ ergs s^{-1} cm^{-2} Hz^{-1} at $d = 50$ kpc (Jura 1974; Draine 1978). The integrated background due to normal, unevolving galaxies is estimated to be log J_ν(1000 Å) $= -21.3$ at $z = 0$ (Dube, Wickes, and Wilkinson 1979; Anderson *et al.* 1979) or $(1 + z)^3$ this value, log J_ν(1000 Å) $= -20.0$ ergs s^{-1} cm^{-2} Hz^{-1} at $z = 1.79$. The Mg I/Mg II and C I/C II ratios are thus consistent with the radiation field above 912 Å expected in a typical spiral galaxy. An additional, substantial source of UV radiation which contributes flux longward of 912 Å, but not shortward of 912 Å, is not consistent with these line ratios and model assumptions. A better limit on the density, however, would lower these limits on log J_ν(1000 Å) and, in principle, could imply a position for these absorbers out of a galactic disk, in a halo.

d) Si II/Si IV *and Local Sources of Ionizing Radiation*

In Figures 14 and 15, we plot log (Si II/Si IV) and log (Si III/Si IV) as a function of ionization parameter for the QSO field described above, and total log N(H I) = 16.5, 17.5, and 18.5, as before. At zero velocity, the observed τ(Si II λ1526)/τ(Si IV λ1403) > 10; since τ(Si II λ1526)/τ(Si IV λ1403) $= 1.05$ N(Si II)/N(Si IV), Figures 14 and 15 imply log $U < -3.5$, and assuming the normalization of the QSO radiation field as above, one derives that log $n > -1.7$ cm^{-3}. Assuming N(C II) $= 5 \times 10^{15}$ cm^{-2} as above, this implies that C II* should have the undetectably small equivalent width of 830 microangstroms.

Applying log $U = -3.5$ to the Mg I/Mg II ratio (Fig. 12) implies that log (Mg I/Mg II) $= -0.5$, a factor of 100 *above* the observed value. Thus, sources of radiation longward of 912 Å other than the QSO field are implied, or else the Mg I absorption would be stronger. The observed log Mg I/Mg II $= -2.5$ and assumed log $U > -3.5$ imply that J_ν(1000 Å) is about 80 times the QSO field, or log J_ν(1000 Å) > -19.9 ergs cm^{-2} s^{-1} Hz^{-1}. Thus, the implied radiation field at 1000 Å, $-19.9 <$ log J_ν(1000 Å) < -19.1 ergs cm^{-2} s^{-1}, is in the range of the expected UV field from a spiral galaxy. Clearly, however, the uncertainties are large, and the result is very model-dependent.

Finally, we note that for log $U = -3.5$, the fraction of hydrogen that is H I is about 0.05. Thus, if log N(H I) < 18.5 cm^{-2}, then log N(H) < 19.8 cm^{-2} and if log $n = -1.7$ cm^{-3}, then the diameter of the cloud is less than 1 kpc. Unreasonably large sizes for these clouds are not implied by these models.

V. CONCLUSIONS

We have obtained echelle spectra of several species of the absorption line system at $z = 1.79$ toward the quasar B2 1225+317. The absorption profiles differ significantly from species to species, with some velocity components absorbing strongly in both low- and high-ionization species, while others show detectable absorption only in C IV and Si IV. The relative column densities of Zn II, Si II, Mg II, Fe II, and H I are, within the uncertainties, consistent with the ratios observed in the interstellar medium.

We interpreted the observed line ratios by constructing photoionization models to derive properties of the radiation field above the Lyman limit at $z = 1.79$. The C II/C II* ratio places a limit on the total density of the absorbing material for components for which C II is detected. This estimate of the density, together with our models for the UV diffuse radiation field from the integrated light of QSOs, then places a lower limit on the ionization parameter. The observed Mg I/Mg II ratio then places an upper limit on the specific intensity at 1000 Å. The observed Si II/Si IV ratio places an upper limit on the ionization parameter, which, with the Mg I/Mg II ratio, implies a lower limit to the specific intensity at 1000 Å. The resulting range is consistent with the expectations for the UV radiation field in the halo of a spiral galaxy.

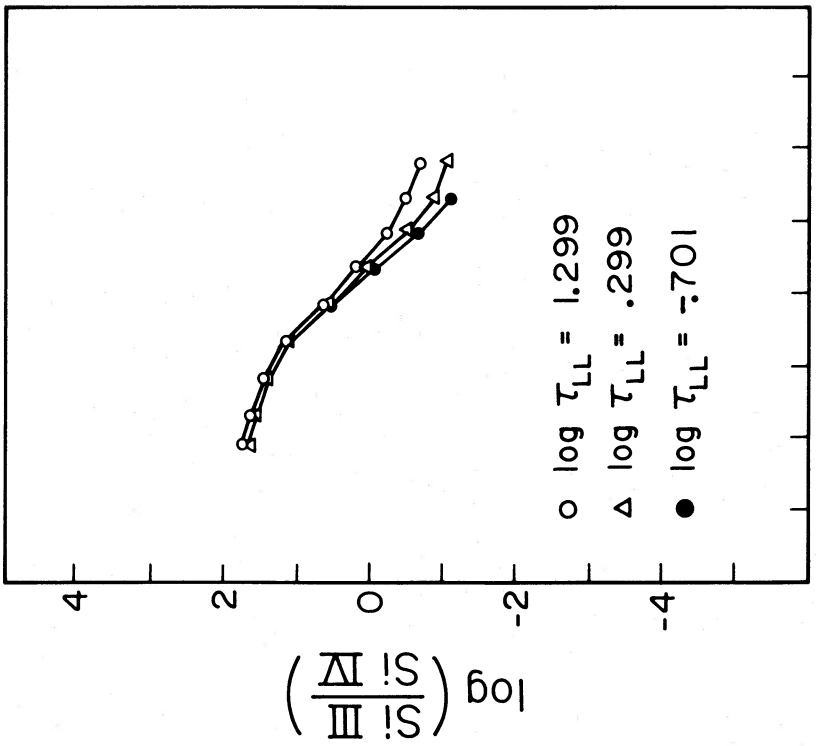

FIG. 15

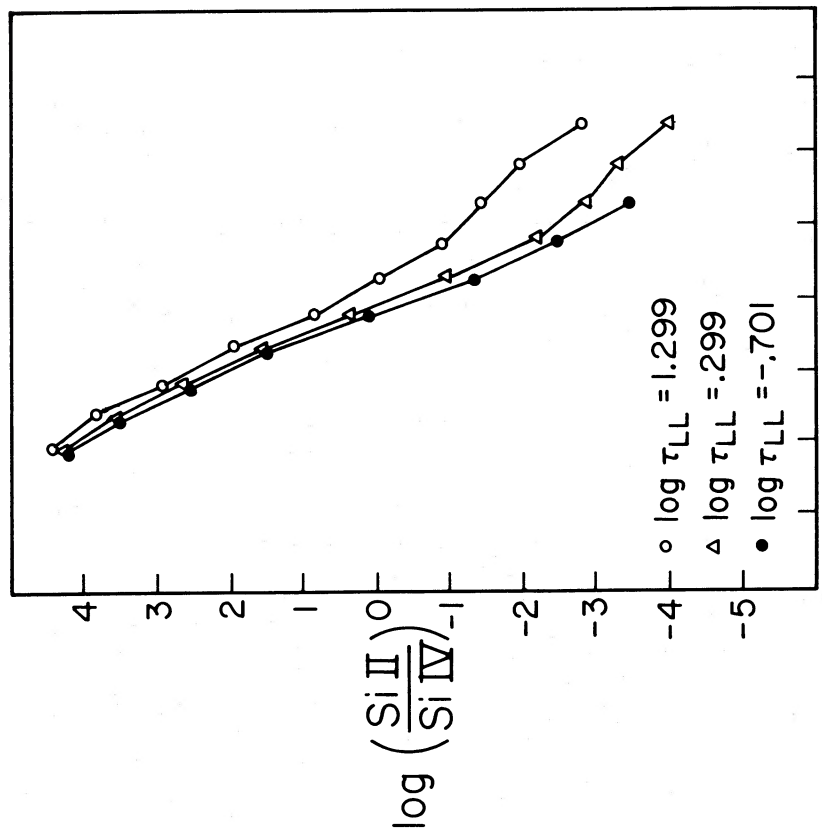

FIG. 14

FIG. 14.—Si II/Si IV as a function of ionization parameter, $z = 1.79$ QSO radiation field
FIG. 15.—Si III/Si IV as a function of ionization parameter, $z = 1.79$ QSO radiation field

We are grateful to Gary Ferland for supplying his photoionization code, CLOUDY, and advice on its use. It is a pleasure to thank the staff of the Multiple Mirror Telescope Observatory for their capable assistance, and the MMT Visitors program and the Steward Observatory for the generous allotment of telescope time. We thank R. Weymann, F. Chaffee, C. Foltz, and J. Black for useful discussions. This work was supported in part by NASA grant NAG 5-38 to the University of Arizona, and NASA grant NAGW 507 to the University of Chicago.

REFERENCES

Anderson, R. C., Henry, R. C., Brune, W. H., Feldman, P. D., and Fastie, W. G. 1979, *Ap. J.*, **234**, 415.
Bahcall, J. N., and Wolf, R. A. 1968, *Ap. J.*, **152**, 701.
Bechtold, J., Green, R. F., Boroson, T. A., Foltz, C. B., Price, C., Schetman, S., and Weymann, R. J. 1986*a*, in preparation (Paper II).
Bechtold, J., Green, R. F., Weymann, R. J., Schmidt, M., Estabrook, F. B., Sherman, R. D., Wahlquist, H. D., and Heckman, T. M. 1984, *Ap. J.*, **281**, 76.
Bechtold, J., Weymann, R. J., Lin, Z., and Malkan, M. A. 1986*b*, *Ap. J.*, submitted.
Bergeron, J., and Boisse, P. 1984, *Astr. Ap.*, **133**, 374.
Biemont, E., and Godefroid, M. 1980, *Astr. Ap.*, **84**, 361.
Blades, J. C., Hunstead, R. W., Murdoch, H. S., and Pettini, M. 1982, *M.N.R.A.S.*, **200**, 1091.
———. 1985, *Ap. J.*, **288**, 580.
Bohlin, R. C., Hill, J. K., Jenkins, E. B., Savage, B. D., Snow, T. P., Spitzer, L., York, D. G. 1983, *Ap. J. Suppl.*, **51**, 277.
Bohlin, R. C., Savage, B. D., and Drake, J. F. 1978, *Ap. J.*, **224**, 132.
Boisse, P., and Bergeron, J. 1985, *Astr. Ap.*, **145**, 59.
Briggs, F. H., Turnshek, D. A., and Wolfe, A. M. 1984, *Ap. J.*, **287**, 549.
Briggs, F. H., and Wolfe, A. M. 1983, *Ap. J.*, **268**, 76.
Bruhweiler, F., Oegerle, W., Weiler, E., Stencel, R., and Kondo, Y. 1984, in *The Future of Ultraviolet Astronomy Based on Six Years of IUE Research*, ed. J. M. Mead, R. D. Chapman, and Y. Kondo (Washington: NASA), p. 200.
Chaffee, F. H. 1974, *Ap. J.*, **189**, 427.
Chaffee, F. H., Foltz, C. G., Bechtold, J., and Weymann, R. J. 1986, *Ap. J.*, **301**, 116.
Chaffee, F. H., Weymann, R. J., Latham, D. W., and Strittmatter, P. A. 1983, *Ap. J.*, **267**, 12.
Cohn, H., and York, D. G. 1977, *Ap. J.*, **216**, 408.
Draine, B. T. 1978, *Ap. J. Suppl.*, **36**, 595.
Dube, R. R., Wickes, W. C., and Wilkinson, D. T. 1979, *Ap. J.*, **232**, 333.
Ferland, G. J. 1981, *Ap. J.*, **249**, 17.
Ferland, G. J., and Truran, J. W. 1981, *Ap. J.*, **244**, 1022.
Fitzpatrick, E. L. 1984, *Ap. J.*, **282**, 436.
Grandi, S. A. 1979, *Ap. J.*, **233**, 5.
Harris, A. W., Bromage, G. E., and Blades, J. C. 1983, *M.N.R.A.S.*, **203**, 1225.
Humlicek, J. 1979, *J. Quant. Spec. Rad. Transfer*, **21**, 309.
Jenkins, E. G., Savage, B. D., and Spitzer, L. 1985, preprint.
Jenkins, E. G., and Shaya, E. J. 1979, *Ap. J.*, **231**, 55.
Jura, M. 1974, *Ap. J.*, **191**, 375.
Latham, D. W. 1982, in *IAU Colloquium 67, Instrumentation for Astronomy with Large Optical Telescopes*, ed. C. M. Humphries (Dordrecht: Reidel), p. 245.
Lugger, P., Barker, E., York, D. G., and Oegerle, W. 1982, *Ap. J.*, **259**, 67.
Morton, D. C. 1978, *Ap. J.*, **222**, 863.
Morton, D. C., and Smith, W. H. 1973, *Ap. J. Suppl.*, **26**, 333.
Murray, M. J., Dufton, P. L., Hibbert, A., and York, D. G. 1984, *Ap. J.*, **282**, 481.
Nussbaumer, H., Pettini, M., and Storey, P. J. 1981, *Astr. Ap.*, **102**, 351.
Pagel, B. E. J. 1986, in *Symposium on Cosmogonical Processes*, ed. W. D. Arnett (Chicago: University of Chicago Press), in press.
Pettini, M., Boksenberg, A., Bates, B., McCaughan, R. F., and McKeith, C. D. 1977, *Astr. Ap.*, **61**, 839.
Pettini, M., Hunstead, R. W., Murdoch, H. S., and Blades, J. C. 1983, *Ap. J.*, **273**, 436.
Pettini, M., and West, K. A. 1982, *Ap. J.*, **260**, 561.
Sargent, W. L. W. 1977, in *The Evolution of Galaxies and Stellar Populations*, ed. B. M. Tinsley and R. B. Larson (New Haven: Yale University Observatory), p. 437.
Sargent, W. L. W., Young, P. J., Boksenberg, A., and Tytler, D. 1980, *Ap. J.*, **42**, 41.
Savage, B. D., and deBoer, K. 1979, *Ap. J. (Letters)*, **230**, L77.
———. 1981, *Ap. J.*, **243**, 460.
Savage, B. D., and Massa, D. 1985, *Ap. J. (Letters)*, **295**, L9.
Shull, J. M., Snow, T. P., and York, D. G. 1981, *Ap. J.*, **246**, 549.
Shull, J. M., and Van Steenberg, M. 1982, *Ap. J. Suppl.*, **48**, 95.
Snijders, M. A. J., Pettini, M., and Boksenberg, A. 1981, *Ap. J.*, **245**, 386.
Ulrich, M.-H. 1976, *Ap. J. (Letters)*, **207**, L73.
Weisheit, J. C. 1978, *Ap. J.*, **219**, 829.
Weymann, R. J., Williams, R. E., Peterson, B. M., and Turnshek, D. A. 1979, *Ap. J.*, **234**, 33.
Wilkerson, M. S., Coleman, G., Gilbert, G., Strittmatter, P. A., Williams, R. E., Baldwin, J. A., Carswell, R. F., and Grandi, S. A. 1978, *Ap. J.*, **223**, 364.
Wolfe, A. M. 1983, *Ap. J. (Letters)*, **268**, L1.
York, D. G. 1982, *Ann. Rev. Astr. Ap.*, **20**, 221.
York, D. G., Dopita, M., Green, R. F., and Bechtold, J. 1986, *Ap. J.*, **311**, 610.
York, D. G., Green, R. F., Bechtold, J., Chaffee, F. H. 1984, *Ap. J. (Letters)*, **280**, L1 (Paper I).
York, D. G., and Jura, M. 1982, *Ap. J.*, **254**, 88.
York, D. G., and Kinahan, B. F. 1979, *Ap. J.*, **228**, 127.
Young, P. J., Sargent, W. L. W., and Boksenberg, A. 1982, *Ap. J. Suppl.*, **48**, 445.

JILL BECHTOLD: Mount Wilson and Las Campanas Observatories, 813 Santa Barbara Street, Pasadena, CA 91101–1292

RICHARD F. GREEN: Kitt Peak National Observatory, NOAO, P.O. Box 26732, Tucson, AZ 85726–6732

D. G. YORK: Department of Astronomy and Astrophysics, University of Chicago, 5640, S. Ellis Avenue, Chicago, IL 60637